AIAA JOURNAL
Vol. 31, No. 8, August 1993

Technical Notes

TECHNICAL NOTES are short manuscripts describing new developments or important results of a preliminary nature. These Notes cannot exceed 6 manuscript pages and 3 figures; a page of text may be substituted for a figure and vice versa. After informal review by the editors, they may be published within a few months of the date of receipt. Style requirements are the same as for regular contributions (see inside back cover).

Some Measurements on Dependence of Rectangular Cylinder Drag on Elevation

R. G. Batt* and S. A. Peabody II†
TRW Space and Defense, Redondo Beach, CA 90278

Introduction

A NUMBER of results for rectangular-shaped bodies have been published on the dependence of drag coefficient on such model/flowfield variables as Reynolds number,[1-3] fineness ratio,[3] corner rounding,[2] and (base) splitter-plate length.[3-5] To date, however, only limited experiments have been conducted wherein drag measurements have been obtained that quantify drag data as a function of elevation, i.e., results for raised rectangular cylinders with an air gap between the model's base plane and the mounting floor. Results, when available, have in turn been restricted to either zero-elevation data (e.g., splitter-plate measurements) or "elevation independent" freestream experiments. Investigators have pointed out the important role of vortex shedding effects on base scavenging, which causes high base drag (low base pressure) for the freestream drag experiments. Conversely, high base pressures experienced by splitter-plate models are consistent with inhibition of vortex shedding due to plate interference effects.

The current documentation summarizes some recent measurements of rectangular cylinder drag on model elevation. All results were obtained with a rectangular-shaped model of 1 in./0.0254 m base height (H) in a laboratory scale shock tube at low shock overpressures ($\Delta P \simeq 7.5$ psi/51.7 kPa) for model elevations (HE) from $HE/H = 0.125$ to 6.00 (freestream). Both "early"-time ($\Delta t \simeq 1.5$ ms) diffraction loads data and "late"-time steady-state results ($\Delta t \simeq 15$ ms) are presented. Although only clean flow (i.e., dust free) data are described herein, additional results regarding drag elevation sensitivity due to berm elevation, shock overpressure, and dusty boundary-layer flow can be found in Ref. 6.

Experimental Technique

The present experiments were performed in TRW's 17 in./0.43 m shock tube. This bursting diaphragm facility incorporates a burst-on-command capability and a long rectangular test section (7 in./0.178 mW × 14 in./0.356 mH × 18 ft./5.49 mL). All results as discussed correspond to tests conducted at a shock overpressure (ΔP) of approximately 7.5 psi/51.7 kPa ($M_e \simeq 0.3$, $Re_{e,H} \simeq 2.5 \times 10^5$) and for test times $\leq$ 15 ms. A single geometric configuration was used for the investigation (1 in./0.0254 mH × 0.625 in./0.0159 mW × 6.75 in./0.1715 mL) corresponding, approximately, to a 0.5% scale model of a typical railroad car design. This model (finess ratio: $w/H \simeq 0.625$) was supported above the shock tube floor by means of adjustable aft support brackets and base-installed force rings. Fences were also mounted on the base to isolate the center span base flow from corner/boundary layer bleed effects. Sensing orifices at the model's centerline on the forward and aft faces permitted alternating sensing direction for a given run pair. Since results for each test condition were obtained by at least one run pair using alternating pressure ports, possible biases in derived pressure drag (impact/base pressure differential) due to minor calibration uncertainties were alleviated. Therefore, all data as shown are averaged drag results based on at least one run pair (using alternating impact/base pressure taps between each individual run). Cabling for the transverse mounted pressure transducers (PCB model 113A21) and the base force rings (quartz force transducer, PCB model 201A02) were brought out from the shock tube interior through sealed side port openings. Electrical and mechanical isolation for the two pressure transducers was maintained throughout the experimental program.

Transducer calibrations were performed prior to and after each shock tube entry. For calibrating the pressure transducers, a special purpose calibrator with a high pressure tank and rapid opening solenoid valve was used. As recommended by the load cell supplier, corresponding force ring calibration data (force loads) were obtained by monitoring individual gauge output upon rapid removal of known imposed weights. Both load rings were pretorqued between precision mounting surfaces to 30 in.-lb/3.39 m-N torque levels prior to testing/calibrating, and antifriction washers were utilized to avoid mounting interference effects. The use of two drag measuring techniques, impact/base differential pressures and load ring "forces," not only permits redundancy in measurement but also provides a means to evaluate dust loading phenomena and relative uncertainties in developing drag data from reliance on centerline tap data alone.

Results

Results from initial shock tube tests, as performed to obtain flash shadowgraphs (exposure time ≤ 5 μs) of shock diffraction patterns for the early-time model flowfield are shown in Fig. 1, for times up to 740 μs after shock passage. For these tests, a solid 0.5% scale model without pressure taps and base fences was suspended 0.25 in./0.00635 m off the floor by use of two slender pylons located 1 in. in from each shock tube side wall. The noted shadowgraph results, which are similar to the higher resolution interferogram measurements of Bleakney et al.,[7] illustrate the nature of the early time shock process and corner vortex motion for this nonsteady flowfield. Such data serve to characterize the sequential development of the base vortices and their subsequent downstream motion in terms of geometrics and timing.

The "characteristic" drag coefficient data reviewed herein include force (CDF), pressure (CDP), base (CDB), and impact (CDI) drag coefficients. These drag CDs are defined as follows:

Force: CDF = $(F_E + F_W)/(HLq_\infty)$, where F_E and F_W represent averaged loads data from the east and west force rings, respectively, H is the model height (1.0 in./.0254 m), L is the model span width (6.75 in./0.1715 m), and q_∞ is the freestream dynamic pressure.

Pressure: CDP = $(P_I - p_B)/q_\infty$. Here P_I and p_B correspond to measured impact and base pressure, respectively.

Base: CDB = $(p_\infty - p_B)/q_\infty$.

Impact: CDI = CDF − CDB.

Received Nov. 14, 1992; revision received Jan. 22, 1993; accepted for publication Feb. 11, 1993.

*Staff Scientist, Propulsion Technology and Fluid Mechanics Center.

†Research Engineer, Propulsion Technology and Fluid Mechanics Center.

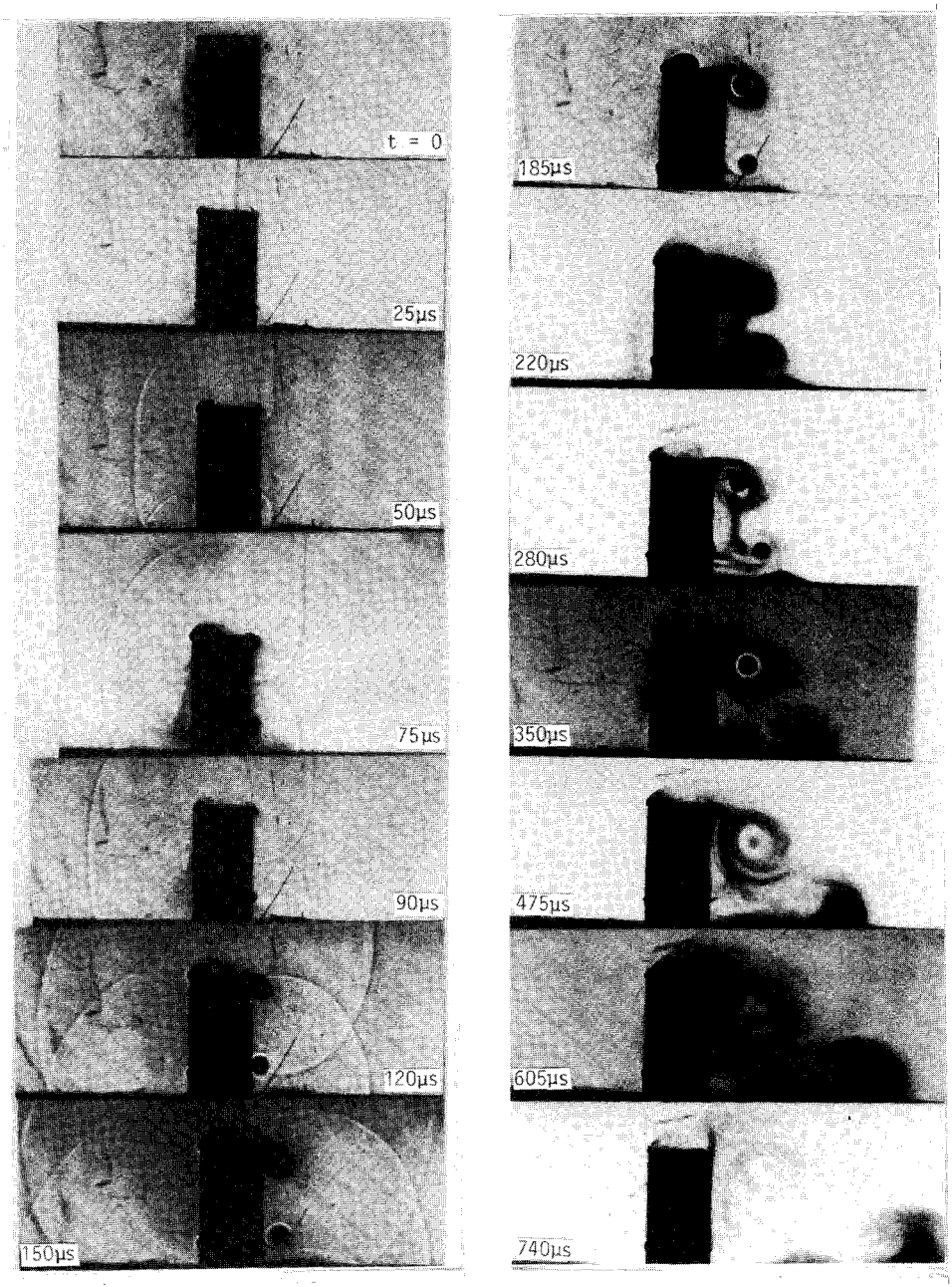

Fig. 1 Shadowgraph photographs of diffraction phase flowfield for elevated rectangular cylinder ($\Delta P \simeq 7.5$ psi/51.7 kPa; 0.25 in./0.00635 m elevation; 1.00 in./0.025 m model base height; 0.625 fineness ratio).

Typical summary plots illustrating the time history behavior for the four noted CDs are given in Fig. 2. The data as shown correspond to clean flow runs without berm at a 7.5 psi shock overpressure test condition and for model elevations of $HE/H = 0.25$ (Fig. 2a) and 6.00 (Fig. 2b). Note that a baseline shift has been applied to the data to accommodate adequate trace separation. The data for the $HE/H = 0.25$ test case are characterized by a relatively large early time (diffraction) drag load ($CDP_D \sim 3.5$), primarily caused by a sharp decrease in base pressure (increase in drag), followed by a decay to a more or less steady-state level ($CDF_{SS} \simeq CDF_{SS} = 1.4$). Corresponding drag data for the $HE/H = 6.00$ case are characterized by negligible diffraction loads but moderately high late-time drag forces ($CD \simeq 3.0$). The numbers noted on the figures represent approximate average values at the indicated times. For both overpressure cases, the late-time data demonstrate that satisfactory correspondence exists between the force and pressure coefficients, thus providing a favorable redundancy check on measured results. Similar drag coefficient summaries for all run pairs considered during the test program are provided in Ref. 6. For all clean flow measurements, the late-time CDF and CDP data are found to be in good agreement.

Figure 3 summarizes for the current investigation the dependence of model drag on elevation under clean flow and berm-free conditions. Data are presented for force drag (CDF), pressure drag (CDP), and base drag (CDB) as a function of elevation height ($0 \leq HE/H \leq 6$). Both early-time diffraction data ($t \simeq 1.5$ ms) and late-time steady-state results ($t \simeq 10$ ms) are indicated. Blockage corrections based on the analysis of Maskel[8] have been applied to the 6 in./0.1524 m elevation data to relate CD magnitudes to undisturbed freestream conditions.

Although several observations regarding the data in Fig. 3 merit consideration, two of the most relevant ones are the substantial reduction in steady-state CD occurring with proximity to the ground surface and the dependence of diffraction drag on elevation. These trends are noteworthy in that drag estimates cannot be based on freestream, i.e., ground independent data, and instead must be determined under realistic ground surface simulation conditions. This dependence is as

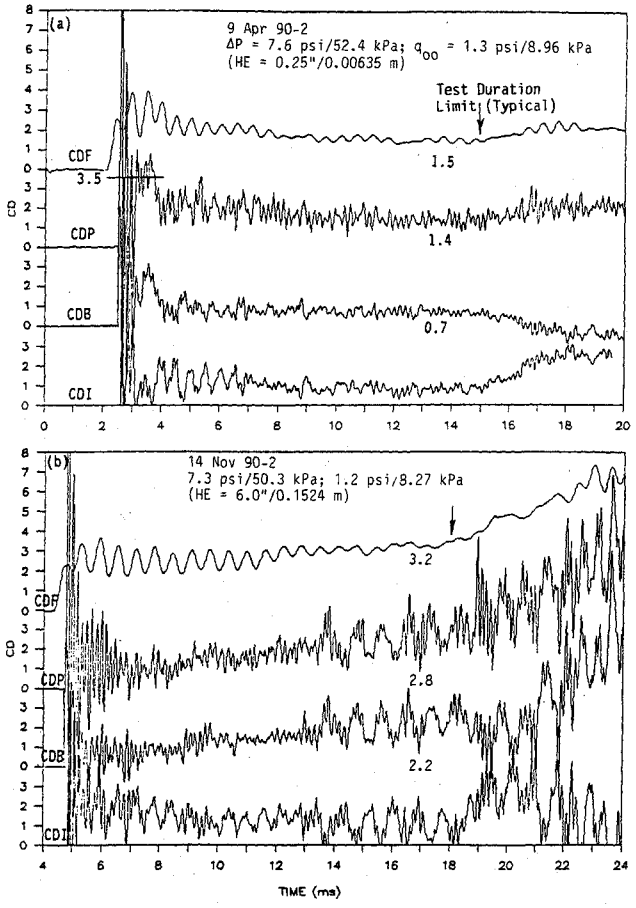

Fig. 2. Typical CD coefficient time histories ($\Delta P \simeq 7.5$ psi/51.7 kPa; clean; without berm).

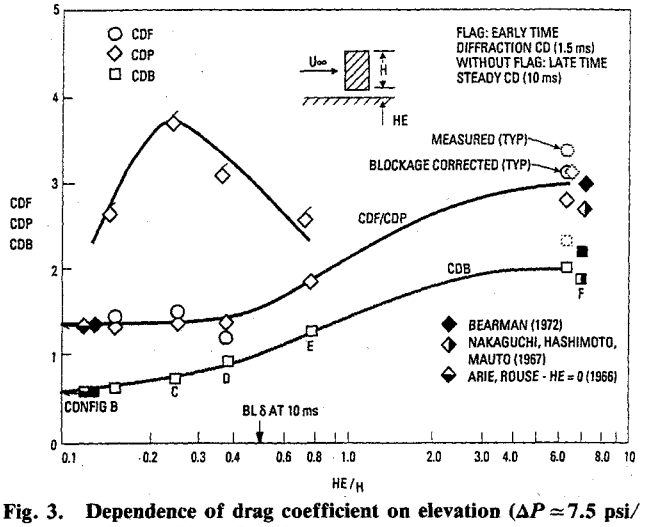

Fig. 3. Dependence of drag coefficient on elevation ($\Delta P \simeq 7.5$ psi/51.7 kPa; clean; without berm).

critical to loads evaluation studies as fineness ratio, Reynolds number, and corner rounding considerations. Note the favorable comparison between the current steady-state data for the two elevation limit cases, $HE \to 0$ and $HE \to \infty$, with earlier results.[3,9,10] Apparently the influence of boundary-layer buildup ($\delta_{10\,ms} \simeq 0.5$ in./0.0127 m) on measured CD results is "small" as demonstrated by the favorable agreement of the low *HE* data with established splitter-plate results. Also, the effects of vortex shedding (evidenced by the presence or absence of periodicity in the CDB data), as already discussed and reviewed by Bearman[5] and Vickery,[11] can be seen to play a major role in maintaining low base pressures (high CDB) at high elevation ($HE/H = 6$, Fig. 2b) and low CDB at low elevation where base scavenging due to vortex shedding is substantially reduced ($HE/H = 0.25$, Fig. 2a).

Because of the sensitivity of base pressure to the vortex shedding phenomena, investigators have pointed out that reduction in base drag can be achieved by modest geometric changes that interfere with the vortex generating mechanism. Such configuration modifications include fineness ratio,[3] corner rounding,[2] splitter-plate length,[3-5] trailing-edge spoiler,[3] and surface proximity (current results). Note, for example, the onset at late time of periodicity in the CDB signal at $HE/H = 6$ in Fig. 2b (the vortex shedding "signature") and the absence of any periodicity for the data for $HE/H = 0.25$ (e.g., Fig. 2a). Since the drag "beat" frequency is typically twice that of the corner shedding frequency,[10] an estimate can be made as to the Strouhal number (S) for the current study

$$S = \bar{n}H/u_{\infty}$$

where $\bar{n}$ represents the Strouhal frequency ($\simeq 0.5 \times$ drag periodicity), H the model height, and u_{∞} the local freestream velocity. The computed value so derived is seen to be somewhat higher (0.15) than previous measurements (0.13) (Ref. 3). The onset of CDB periodicity is also consistent with the observed increase in base drag as would be expected since base scavenging is controlled by the establishment of the von Kármán vortex street.[3,4]

References

[1]Lindsey, W. F., "Drag of Cylinders of Simple Shapes," NACA Rept. 619, 1938.

[2]Delany, N. K., and Sorensen, N.E., "Low-Speed Drag of Cylinders of Various Shapes," NACA TN 3038, Nov. 1953.

[3]Bearman, P. W., and Trueman, D. M., "An Investigation of the Flow Around Rectangular Cylinders," *Journal of Aeronautical Quarterly*, Vol. 23, Pt. 3, Aug. 1972, pp. 229-237.

[4]Roshko, A., "On the Wake and Drag of Bluff Bodies," *Journal of the Aeronautical Sciences,* Vol. 22, No. 2, 1955, pp. 124-132.

[5]Bearman, P. W., "Investigation of the Flow Behind a Two-Dimensional Model with a Blunt Trailing Edge and Fitted with Splitter Plates," *Journal of Fluid Mechanics,* Vol. 21, Pt. 2, 1965, pp. 241-255.

[6]Batt, R. G., and Peabody, S. A., II, "Rail Garrison Instrumentation Development," Defense Nuclear Agency, DNA-TR-91-126, Dec. 1991.

[7]Bleakney, W., White, D. R., and Griffith, W. C., "Measurements of Diffraction Shock Waves and Resulting Loading of Structures," *Journal of Applied Mechanics,* Vol. 17, No. 4, 1950, pp. 439-445.

[8]Maskel, E.C., "A Theory of the Blockage Effects on Bluff Bodies and Stalled Wings in a Closed Wind Tunnel," Aeronautical Research Council, Great Britain, Repts. and Memoranda No. 3400, Nov. 1965.

[9]Nakaguchi, H., Hashimoto, K., and Muto, S., "An Experimental Study on Aerodynamic Drag of Rectangular Cylinders," *Journal of the Japan Society of Aeronautical and Space Sciences,* Vol. 16, No. 1, 1968, pp. 1-5.

[10]Arie, M., and Rouse, H., "Experiments on Two-Dimensional Flow over a Normal Wall," *Journal of Fluid Mechanics,* Vol. 1, Pt. 2, 1956, pp. 129-141.

[11]Vickery, B. J., "Fluctuating Lift and Drag on a Long Cylinder of Square Cross-Section in a Smooth and in a Turbulent Stream," *Journal of Fluid Mechanics,* Vol. 25, Pt. 3, 1966, pp. 481-494.

Fluid Column Stability in the Presence of Periodic Accelerations

M. J. Lyell*
West Virginia University, Morgantown, West Virginia 26506

Introduction

THE float zone configuration is used in crystal growth. It may be modeled as a liquid column held by surface ten-

Received Sept. 21, 1992; revision received Jan. 20, 1993; accepted for publication Jan. 24, 1993.

*Associate Professor, Mechanical and Aerospace Engineering Department. Senior Member AIAA.